UCRL-JRNL-234716

LAWRENCE
LIVERMORE
NATIONAL
LABORATORY

Measurement and Modeling of Inner-Shell Satellites of Na-like Fe XVI between 14.5 Å and 18 Å

A. Graf, P. Beiersdorfer, G. V. Brown, M. F. Gu

September 18, 2007

Astrophysical Journal

Disclaimer

This document was prepared as an account of work sponsored by an agency of the United States Government. Neither the United States Government nor the University of California nor any of their employees, makes any warranty, express or implied, or assumes any legal liability or responsibility for the accuracy, completeness, or usefulness of any information, apparatus, product, or process disclosed, or represents that its use would not infringe privately owned rights. Reference herein to any specific commercial product, process, or service by trade name, trademark, manufacturer, or otherwise, does not necessarily constitute or imply its endorsement, recommendation, or favoring by the United States Government or the University of California. The views and opinions of authors expressed herein do not necessarily state or reflect those of the United States Government or the University of California, and shall not be used for advertising or product endorsement purposes.

Measurement and Modeling of Inner-Shell Satellites of Na-like Fe XVI between 14.5 Å and 18 Å

A. Graf

Physics Department University of California-Davis, 1 Shields Avenue, Davis, CA 95616

and

P. Beiersdorfer, G. V. Brown, M. F. Gu

University of California Lawrence Livermore National Laboratory, 7000 East Avenue, Livermore, CA 94550

Received _____; accepted _____

This work was performed in part under the auspices of the U.S. Department of Energy by University of California, Lawrence Livermore National Laboratory under Contract W-7405-Eng-48.

ABSTRACT

We have used the University of California Lawrence Livermore National Laboratory's EBIT-I electron beam ion trap to perform measurements of the wavelengths and relative intensities of the X-ray lines from inner-shell satellite transitions in sodium-like Fe XVI. The measurements were carried out with high-resolution crystal and grating spectrometers and covered the 14.5 - 18 Å wavelength band. Contrary to predicted line strengths and positions found in the literature, our results show that the strongest inner-shell satellites of Fe XVI are located near 15.2 Å. This is near the location of the 3d→2p intercombination line in Fe XVII. Calculations using the Flexible Atomic Code are presented, which agree well with the EBIT-I measurements.

Subject headings: atomic data—line: X-rays general, identification, ratio

1. Introduction

In a multitude of astrophysical X-ray sources, the wavelength band between 10 and 18 Å is rich with X-ray line emission including strong lines from Fe L-shell transitions in Fe XVII-XXIV. It may also contain emission from levels with high principal quantum number in O VII and O VIII as well as the K-shell transitions of Ne IX and Ne X. The most distinct lines are typically from the 3d→2p and 3s→2p transitions in Fe XVII at ∼15 and ∼17 Å, respectively. Several observational, experimental, and theoretical studies of the Fe XVII emission in this band have been completed (Parkinson 1973; Loulergue & Nussbaumer 1973; Brown et al. 1998; Gu 2003; Beiersdorfer et al. 2004). Moreover, a catalogue of the L-shell transitions of Fe XVIII through Fe XXIV was established in the laboratory (Brown et al. 2002; Chen, H. et al. 2007) and compared to novel calculations using many body perturbation theory (Gu 2005).

The X-ray emission from the relatively weaker inner-shell (IS) satellite transitions in Na-like Fe XVI that fall in this wavelength band have not been as well studied even though they have been identified in cool sources such as the quiet Sun and the corona of Procyon (Raassen et al. 2002). Further, it has been shown by Brown et al. (2001) and Behar et al. (2001) that the IS satellites from Fe XVI can significantly change relative line strengths of some of the strongest lines in Fe XVII as a result of line blending. This effect has subsequently been reinforced by Brickhouse & Schmelz (2006) in their analysis of solar X-ray spectra. The Fe XVI line strengths must therefore be known and taken into account, lest the accuracy of the spectral diagnostics in this wavelength band are compromised.

The Fe XVI IS satellite X-ray spectrum which falls in the wavelength band between 14.5 and 18 Å has been calculated by several authors, including Cornille et al. (1994) and Phillips et al. (1997). Neither the relative line intensities nor the wavelengths predicted by these calculations agree with each other casting doubt on the modeling of the strength,

and in principle on the identification of Fe XVI IS satellites in a spectrum measured from celestial sources.

To provide accurate wavelengths and relative line intensities and to discriminate among different modeling calculations, we have measured the X-ray emission from Na-like Fe XVI under controlled and well known conditions using the University of California Lawrence Livermore National Laboroatory's (LLNL) EBIT-I facility. Here we present the results of our measurement and compare them with the published theories of Cornille et al. (1994) and Phillips et al. (1997); as well as our own new calculation using the Flexible Atomic Code (FAC).

2. Experiment

The LLNL EBIT-I electron beam ion trap has been used extensively for laboratory astrophysics (Beiersdorfer et al. 2003). EBIT-I uses a mono-energetic electron beam to ionize neutral material, excite bound electrons, and trap ions radially. Along the electron beam direction, ions are trapped by different potentials applied to three surrounding drift tubes. The length of the trap along the electron beam is 2 cm. The diameter of the electron beam is $\sim$50 μm, removing the need for an entrance slit for dispersive spectrometers. A detailed description of the LLNL electron beam ion traps is given in Beiersdorfer et al. (2003) and Marrs (1995).

To study the effects of Fe XVI IS satellites on Fe XVII line emission in the 14.5 - 18 Å wavelength band one must use an an electron beam energy greater than $\sim$830 eV. For the measurement presented here, we used an electron beam energy of 1.10$\pm$ 0.03 keV which means lines with wavelength as short as 11 Å can be excited. This energy is well above the 489 eV ionization energy of Fe XVI, and in collisional ionization equilibrium, essentially

no Fe XVI exist at this beam energy. For our measurement, a relatively large population of Fe XVI ions is sustained by continually introducing iron into the trap in the form of the neutral molecular gas, iron pentacarbonyl, $Fe(CO)_5$, with a ballistic gas injector. The continuous injection of neutral iron results in an underionized plasma, and thus a lower ionization balance. This is the same method used by Brown et al. (2001).

We employed two spectrometers to observe the X-ray spectrum: a broadband flat crystal spectrometer (Brown, et al. 1999) and a flat-field, grazing-incidence reflection grating spectrometer (Beiersdorfer et al. 2004). The spectrum measured with the grating spectrometer is shown in Fig. 1a. Spectra obtained with the crystal spectrometer are shown in Figs. 2 and 3, which are also overlaid with the grating data. The flat crystal spectrometer uses a rubidium acid phthalate (RAP, 2d = 26.121 Å) crystal for diffraction and a position sensitive proportional counter (PSPC) for detection. The proportional counter uses P-10 gas (90% Ar and 10% CH_4) at a pressure of 760 torr as a detection gas. The crystal spectrometer has ∼3 Å bandpass and a resolving power of $\lambda/\Delta\lambda$ ∼600 for λ in the 14.5 - 18 Å band. The absorption of X-rays by air in the spectrometer is eliminated by operating at a pressure below 2 x 10^{-7} torr. This is much higher than the maximum pressure in EBIT-I of 10^{-11} torr. To avoid contamination of the vacuum of EBIT-I by the residual gas in the spectrometer, the two chambers are separated by a 0.5 μm thick, free-standing polyimide window. Similarly, a 1 μm thick polyimide window coated with ∼200 Å of aluminum and supported by gold coated tungsten wires (Beiersdorfer et al. 2004), is used to isolate the pressure in the detection chamber (760 torr) of the PSPC from the vacuum of the spectrometer.

The grating spectrometer uses a variable-line-spacing, gold-coated grating to disperse the spectrum onto a flat field. The average line spacing of the grating is 2400 l/mm and it operates at an incident angle of 1.3°. X-rays are detected using a two-dimensional

back-illuminated charge-coupled detector (CCD) with a flat instrumental response between 11 and 19 Å (Beiersdorfer et al. 2004). The bandpass is ∼7 Å with a resolving power of ∼600 for λ in the 14.5 - 18 Å band. The gas load of the spectrometer ($\sim 10^{-7}$ torr) on the EBIT-I vacuum chamber is reduced by a series of baffles between the grating and trap region. No vacuum windows of any kind are used for the grating spectrometer.

2.1. Wavelength Measurement and Line Identification

The wavelength scale of each spectrometer is calibrated using the well known transition wavelengths of hydrogenic O VIII and helium-like O VII, as well as the Ne-like Fe XVII lines, 3C, 3D, 3F, 3G and M2 measured by Brown et al. (1998). The wavelength of O VIII Ly_β was taken from Garcia & Mack (1965). The wavelengths of K_β and K_γ in O VII are given by Vainshtein & Safranova (1985). These have been adjusted by the more accurate calculation of the O VII $1s^2$ ground state energy by Drake (1988). The injection of CO_2 into the trap allowed the measurement of the oxygen calibration spectra.

For the crystal spectrometer the angle that the crystal makes with the incident radiation from EBIT-I determines the wavelength that is reflected according to Bragg's law,

$$n\lambda = 2dsin\theta \tag{1}$$

where n is the order of reflection, λ is the wavelength reflected, d is the crystal lattice spacing and θ is the Bragg angle. The centroids of each line were fit with a Gaussian function in channel space on the PSPC. A linear regression can then be formed between the centroid channel number and expected Bragg angle allowing the production of a wavelength scale. Though the dispersion process for the grating spectrometer is different the wavelength calibration is accomplished in a similar way. In particular, a second order polynomial fit between known wavelength and channel number is used to establish the

wavelength scale. The order of the polynomial was chosen such that the difference between reference wavelengths and those obtained by the calibration is minimized, while ensuring that the distribution of the residuals around zero is random.

The error in the wavelength is the quadrature sum of the error associated with the calibration scale and that from the fit of the centroid. The error from fitting the centroid includes the statistical contribution from the number of counts in the feature. Since the lines of interest are relatively weak we find that the error from fitting the lines is comparable to the error from the the calibration scale. The largest deviation between known calibration line wavelength values and those inferred from the resulting wavelength scale is 3 mÅ while the largest error from fitting the Fe XVI features themselves is 10 mÅ. There is the caveat that if the identified feature is a blend, the wavelength error increases to the maximum separation of the predicted FAC line positions. The largest error in this case is 20 mÅ. The inferred wavelengths of the observed Fe XVI IS satellites from experiment are given in are given in Table 1 column 2.

2.2. Relative Line Intensity

A Gaussian line profile fit to each line is used to determine its intensity. The term intensity is used here loosely to represent the number of photons in a given feature. This has no consequence in the following since we are concerned with line ratios and not absolute values. The width of the Gaussian is determined by an average of widths of isolated X-ray lines. This width is instrument specific and determined separately for the grating and crystal spectrometers. After the average is determined, this single value is used in all of the data analysis from the respective instruments. Many of the Fe XVI IS satellites, especially on the long wavelength end of the spectrum are unresolved blends. The spectrum created using the results from FAC is qualitatively similar to the experiment. This acts as an aid in

choosing the number and wavelength position of Gaussians used for fitting unresolved line features. In each case the optimum result is to fit the blend with the number of features predicted by FAC. This is not always possible for the fitting routine when lines are very close. If the fit represents more than one identified feature then the intensity determined from the fit is compared to the sum of the intensities of the lines predicted by FAC. Columns 7 and 8 contain the line ratio results from FAC for the individual features and their total, respectively.

To compare our measured line intensities to theory and spectra collected from celestial sources, the energy dependent response of the spectrometers must be taken into account. For the crystal spectrometer, this includes the transmission efficiency of the foils isolating the spectrometer chamber from EBIT-I, the reflectivity of the crystal, and the absorption efficiency of the detector gas. Using the data on the Center for X-Ray Optics (CXRO) web-site[1] for transmission and absorption curves, broadband intensity corrections have been made to the spectra. Reflectance from the crystal is taken into account by averaging the values given by the Lorentzian and mosaic models provided by Henke et al. (1993) specific to an RAP crystal. There were no absorption edges encountered for any of the materials in question in this region of the spectrum. While the transmission, absorption and reflectance curves were taken from calculation and not measured directly, they have been shown to be in agreement with the values measured previously (Savin et al. 1996). Since the grating spectrometer has a flat instrumental response in the wavelength region under study (Beiersdorfer et al. 2004), no further efficiency corrections are necessary for obtaining accurate normalized line intensities.

In addition to the corrections above, the anisotropy of emitted line radiation produced in an EBIT must be taken into account. This anisotropy results from the directionality

[1]http://www-cxro.lbl.gov/

of the beam which can cause a symmetric (m_{-J}=m_{+J}) population imbalance of magnetic sublevels leading to a possible linear polarization of the X-ray emission (Beiersdorfer et al. 1996). It can be accounted for by the following:

$$I = \left(\frac{3-P}{3}\right) I\left(90^{\circ}\right), \tag{2}$$

where P, is the polarization of the transition of interest, I(90°), is the line intensity emitted at 90° to the electron beam direction, and I is the total emitted intensity in 4π steradians. This correction is necessary for both spectrometers because they collect light only perpendicular to the beam and not an average over 4π steradian. The form of Eq. 2 is specific to electric dipole transitions only and is appropriate for all but one (feature 9a is a magnetic dipole or M2 transition) of the Fe XVI features identified in this paper. Since the intensity correction for the M2 line cannot be written in a general form it is not shown here.

In the case of the crystal spectrometer, a second additional correction must be included because the crystal acts as a polarimeter preferentially reflecting light polarized perpendicular to the dispersion plane. The relationship between the measured intensity from the crystal spectrometer and the polarization free, isotropically emitted intensity, can be written as follows (Wargelin 1993),

$$I = \left(\frac{3-P}{3}\right)\left[\left(\frac{2}{R_{\parallel}}\right)\frac{1}{\left(1+P+(1-P)\left(\frac{R_{\perp}}{R_{\parallel}}\right)\right)}\right] I\left(90^{\circ}\right), \tag{3}$$

where $R_{\parallel}$ and $R_{\perp}$, are the parallel and perpendicular crystal reflectivities given by Henke et al. (1993).

Equations 2 and 3 require the knowledge of the polarization for the transitions of interest. The polarizations were calculated using FAC and take into account cascading from levels with principal quantum number $n \leq 4$. A neglected effect in the calculation of the polarization is a depolarization that results from a transverse electron velocity within the beam produced by cyclotron motion of the electrons perpendicular to the magnetic field

lines as they travel through the trap (Gu et al. 1999). The polarization changes by up to 20% but the effect on the line ratios is <1%. A more detailed account of the corrections given by equations 2 and 3 are covered in detail by Beiersdorfer et al. (1996), Vogel (1992), and Wargelin (1993), as adapted from the Steffen and Alder (1975) treatment for gamma rays.

The measured line intensities, normalized to the Fe XVI line 2b and corrected for spectrometer effects, discussed above, are given in Table 1 columns 5 and 6. The error in the normalized line intensities results from a quadrature sum of two errors, including that from the baseline fitting for the background subtraction and the statistical error from fitting the line shapes. For the crystal data an extra source of error was included from broadband reflectance and transmission corrections ($\sim$ 6% of the intensity). Any error introduced from not knowing the exact polarization of specific lines is not taken into account. The maximum estimated error is 9% . Also included in Table 1 column 9, are the polarizations as calculated by FAC.

3. Comparison to Theory

In Table 1 our measurements are compared to a simulation based on atomic data computed with FAC version 1.0.9, developed by M. F. Gu [2]. Specifically, a synthetic spectrum of Fe XVI between 14.5 Å and 18 Å was calculated. For a mono-energetic electron beam with an energy of 1.1 keV impinging on iron atoms, electron impact excitation followed by radiative cascades, as well as autoionization into the ground state of Ne-like Fe XVII, are the processes that determine the line strengths of the Fe XVI X-ray lines in this band. Since the beam energy is well above any threshold for dielectronic recombination of Fe XVII

[2]http://kipac-tree.stanford.edu/fac/

for the region of interest, the Fe XVI spectrum is comprised of solely inner-shell satellites. The atomic structure and line formation calculations by FAC are fully relativistic and use the distorted wave approximation for interaction with continuum states. Autoionization of Fe XVI from $2s2p^63l^2, 2p^53l^2, 2s2p^63l4l'$, and $2p^53l4l'$ with l and l'=0,1,2 into the ground state of Fe XVII is included. These model calculations create 242 energy levels which result in nearly 30000 transitions. When the synthetic spectrum is broadened to simulate the data, 10 Fe XVI features with a relative intensity greater than 0.02 are found in the 14.5 - 18 Å bandwidth. The transitions which shape these features having a relative intensity greater than 0.01 are listed in Table 1 column 7. The wavelengths predicted by FAC were typically long by as much as 50 mÅ. The largest deviation being at the longest wavelength. For clarity, the spectrum produced using the results from FAC have been shifted in Figures 2 and 3. The unshifted spectrum can be seen in Figure 1. The function necessary to shift the wavelength values for pictorial comparison was unfortunately non-linear. In fact it was different for the short (2nd order polynomial) and long (Sigmoid) wavelength regions. The unshifted wavelength values from FAC are given in Table 1 column 3.

We note that the line 9a is identified to an M2 (magnetic quadrapole) transition between $2p^62p_{3/2} \rightarrow 2p^2_{1/2}2p^4_{3/2}3s13p_{3/2}$ (J=7/2). Normally, forbidden innershell transitions are rarely observed, because of the large autoionization rate of their upper levels. However, in this particular case, the $2p^2_{1/2}2p^4_{3/2}3s13p_{3/2}$ (J=7/2) level has a very small autoionization rate of 3.6E4 s^{-1}, while the M2 transition rate is calculated to be 1.7E5 s^{-1}, making this line a strong feature.

For comparison between calculations, we also include in Figure 1 predictions of the Fe XVI IS satellites from Cornille et al. (1994) and from Phillips et al. (1997) under similar conditions. Cornille used SUPERSTRUCTURE (Eisner et al. 1974) to calculate the energy levels and radiative transition rates along with DISWAV (Eisner et al. 1972), JAJOM

(Saraph 1972) and JJOMCBE to calculate collision strengths. The autoionization rates come from the code AUTOLSJ (Dubau & Loulergue 1981). The Fe XVI configurations included in the calculation are $2p^6 3s$, $2p^5 3s^2$, $2p^5 3s3p$ and $2p^5 3s3d$, making a total of 44 levels and resulting in ∼12-15 resolvable features. The line emmisivities were determined for an electron impact energy of 816 eV (60 Ry) at an electron density $< 10^{12}$ cm^{-3}. Phillips et al. (1997) used the same computational scenario except the collision strengths were calculated using DSTWAV (Burke & Eisner 1983) at an electron temperature of 843 eV (62 Ry) and a density of 10^8 cm^{-3}. The predicted wavelengths roughly match those given by the Hartree-Fock code with relativistic corrections written by Cowan (1981) and used by Phillips et al. (1997).

Comparing the predictions of Cornille et al. (1994) and Phillips et al. (1997) with our measurements and calculations we note that there is a drastic difference both for relative intensity and line position. Most importantly both calculations predict strong, well resolved lines near 17 Å . In particular, Cornille et al. (1994) predict well resolved lines at 16.6 and 16.7 Å ; Phillips et al. (1997) predict strong lines at 17.0 and 17.3 Å . These lines would serve as a diagnostic for the Fe XVI abundance in the plasma, if the lines were indeed as strong as predicted. Our measurements and FAC calculations show that these lines are neither at these positions nor strong.

Finally, we make a comparison between the calculated relative intensities from FAC and those from experiment for a few of the larger Fe XVI features (Figure 4). The experimental data from the grating and crystal spectrometers tend to agree to within 10% . Unfortunately there are five features from the crystal data which could not be fit properly because of line blending and poor statistics. There is agreement between FAC and experiment for features 2a, 4, 5, and 9a. Otherwise the results from FAC tend to be smaller by a factor of at most 1/0.15. It should be noted that the same FAC results calculated for a smaller beam

energy progressively enhanced the longer wavelength features until the ionization threshold was reached. The lower values of the long wavelength line intensities from FAC could be attributed to the difficulty of accurate calculations of branching ratios when including the 3s, 3p and 3d family of energy levels. The true reason for the predominantly lower results from FAC are unknown. Despite this difference the qualitative agreement to experiment is quite good. There is also a qualitative agreement between our results and the independent calculation and measurement of Brown et al. (2001) represented by the stars in Figure 4. The predicted value of feature 3 is a factor of ∼1/.10 higher than our result. This difference is probably because the line blend of feature 2 (i.e 2a and 2b) was not accounted for in Brown et al. (2001). Treating 2a and 2b as a single line increases its area and thus decreases the relative line strength of feature 4. It should be noted that blending of K_δ from O VII, with feature 6a and 6b at ∼17.38 Å has been taken into account for the grating and crystal data. In each case the oxygen spectrum is normalized to K_γ. The spread in the data combined with the results from FAC show the normalized line intensities presented here to be good to within 20%.

As an application of our results we consider the common diagnostic line ratio from Fe XVII of 3C arising from the $2p^5 3d\ ^1P_1 \rightarrow 2p^6\ ^1S_0$ transition to 3D arising from the $2p^5 3d\ ^3D_1 \rightarrow 2p^6\ ^1S_0$ transition (at 15.01 and 15.26 Å, respectively). Polarization and reflectivity corrections were made to the data from both spectrometers using a polarization of 0.4 (Utter et al. 1999; Zhang et al. 1990; Beiersdorfer et al. 2002) for both 3C and 3D. When the blending of Fe XVI feature 3 with 3D is not accounted for, we find ratios of 2.75±0.19 and 2.29±0.21 for the grating and crystal data, respectively. When the blending is accounted for, the two values increase to 3.05±0.23 and 2.82±0.32 which are in good agreement with the value reported by Brown et al. (1998). While the ratio results don't quite agree with each other before the removal of the blend from feature 3, they agree well with each other after taking the (polarization-dependent) blend into account. Moreover,

the blended ratios are are in decent agreement with that from Brown et al. (2001) for the Fe XVI to Fe XVII relative abundance of ~ 0.2 in our experiment. As noted earlier (Brown et al. 2001; Behar et al. 2001), when using the line ratios I_{3C}/I_{3D} in astrophysical spectra, it is important to account for the presence of Fe XVI satellite emission. If possible, this can be done by first identifying the presence of the strongest Fe XVI feature at 15.20 Å and then normalizing the intensity of the rest of the Fe XVI lines to this feature using the now validated calculation of FAC. Using this method, one can account for both the Fe XVI line coincident with Fe XVII 3C and the weaker Fe XVI contributions to the 3s→2p Fe XVII lines around 17 Å .

4. Conclusion

We have used the LLNL electron beam ion trap, EBIT-I, with high resolution crystal and grating spectrometers to measure the wavelengths and normalized line intensities of some of the larger inner-shell satellites from Fe XVI between 14.5 and 18 Å at a single beam energy of 1.1 keV. Accurate knowledge of these features as a function of temperature and wavelength is necessary for proper evaluation of the diagnostics associated with more prominent X-ray lines in this region. Specifically, line ratio diagnostics using features from Fe XVII including 3D at 15.26 Å or the three major 3s→2p lines around 17 Å may need to account for blending with the Fe XVI IS satellites (dependent on the spectral resolution of the instrument, and the charge state distribution of the source).

The predictions of the relatively strong lines by Phillips et al. (1997) and by Cornille et al. (1994) near 16.5 Å are not confirmed by our measurements. These lines should, thus, not be used as indicators of the presence of Fe XVI IS satellite line emission. Instead, the strongest unblended indicator is the 15.20 Å line, feature 2b in Table 1.

We find a qualitative agreement between our measurement and the synthetic spectrum from FAC. The wavelengths deduced from FAC are slightly long and with a difference which increases with wavelength to a maximum of 50 mÅ. The line ratios for features 2a, 4, 5, and 9a show a quantitative agreement with experiment. Otherwise the line ratio results from FAC tend be lower by factor of at most 1/0.15. The predicted line ratio of feature 4 at 15.26 Å, which is typically a blend with 3D from Fe XVII, is in agreement with the value predicted in Brown et al. (2001).

Finally, for the relative abundance of Fe XVI/Fe XVII $\sim$ 0.2, we find an apparent ratio, I_{3C}/I_{3D}, of 2.75±0.19 and 2.29±0.21 for the grating and crystal spectrometers, respectively. These ratios agree with the results of Brown et al. (2001). When Fe XVI line 3 is accounted for, the ratios of I_{3C}/I_{3D} become 3.05±0.23 and 2.82±0.32 which agree with the result from Brown et al. (1998).

The work at Lawrence Livermore National Laboratory was performed under the auspices of the Department of Energy under Contract W-7405-ENG-48 and supported by the Astronomy and Physics Research and Analysis Program of the National Aeronautics and Space Administration (NASA) under contract S-06553-G.

REFERENCES

Beiersdorfer, P. & Wargelin, B. J. 1994, Rev. Sci. Instrum., 65, 13

Beiersdorfer, P., Vogel, D. A., Reed, K. J., Decaux, V., Scofield, J. H., Widman, K., Hölzer, G., Förster, E. , Wehrhan, O., Savin, D. W. & Schweikhard, L. 1996, Phys. Rev. A, 53, 6, 3974

Beiersdorfer, P., Behar, E., Boyce, K. R., Brown, G. V., Chen, H., Gendreau, K. C., Gu, M. -F., Gygax, J., Kahn, S. M., Kelley, R. L., Porter, F. S., Stahle, C. K., & Szymkowiak, A. E., 2002, ApJ, 576, L169

Beiersdorfer, P., Behar, E., Boyce, K. R., Brown, G. V., Chen, H., Gendreau, K. C., Graf, A., Gu, M. -F, Harris, C. L., Kahn, S. M., Kelley, R. L., Lepson, J. K., May, M. J., Neill,P. A.,Pinnington, E. H., Porter, F. S., Smith, A. J., Stahle, C. K., Szymkowiak, A. E., Tillotson, A., Thorn, D. B., Träbert, E. & Wargelin, B. J. 2003 Nuclear Instruments and Methods in Physics Reseach, Section B, 205, 173

Beiersdorfer, P., 2003, ARAA, 412, 343

Beiersdorfer, P., Bitter, M., von Goeler, S. & Hill, K. W. 2004, ApJ, 610, 616

Beiersdorfer, P., Magee, E. W., Träbert, E., Chen, H., Lepson, J. K., Gu, M. -F., & Schmidt, M. 2004, Rev. Sci. Instrum., 75, 10, 3723

Beiersdorfer, P., Brown, G. V., Goddard, R., & Wargelin, B. J. 2004, Rev. Sci. Instrum., 75, 10, 3720

Behar, E., Cottam, J. & Kahn, S. 2001, ApJ, 548, 966

Brickhouse, N. S. & Schmelz, J. T., 2006, ApJ, 636, L53

Brown, G. V., Beiersdorfer, P., Liedahl, D. A., Widmann, K., & Kahn, S. M. 1998, ApJ, 502, 1015

Brown, G. V., Beiersdorfer, P., & Widmann, K. 1999. Rev. Sci. Instrum., 70, 1, 280

Brown, G. V., Beiersdorfer, P., Chen, H., Chen, M. H., & Reed, K. J. 2001, ApJ, 557, L75

Brown, G. V., Beiersdorfer, P., Liedahl, D. A., Widman, K., Kahn, S. M., and Clothiaux, 2002, E. J., ApJS, 140, 589

Burke, P. G. & Eisner, W. 1983, *Atoms in Astrophysics*, (Plenum Press, New York)

Chen, H., Gu, M. F., Behar, E., Brown, G. V., Kahn, S. M., and Beiersdorfer, P., 2007 ApJS, 168, 319

Cornille, M., Dubau, J., Faucher, P., Bely-Dubau, F. & Blancard, C. 1994, A&A Suppl. Ser., 105, 77

Cowan, R. D. 1981 *The Theory of Atomic Structure and Spectra*, (Berkeley: Univ. Colorado Press)

Dubau, J. & Loulergue, M. 1981, Phys. Scr., 23, 136

Drake, G. W. 1988, Can. J. Phys., 66, 586

Eisner, W. & Seaton, M. J. 1972, J. Phys. B, 5, 2187

Eisner, W., Jones, M. & Nussbaumer, H. 1974, Comp. Phys., 8, 270

Garcia, J. D. & Mack, J. E. 1965, Journal of the Optical Soc. of America, 55, 6, 654

Gu, M. F., Beiersdorfer, P., & Savin, D. W. 1999, J. Phys. B, 32, 5371

Gu, M. F. 2003, ApJ, 582, 1241

Gu, M. F. 2005, ApJS, 156, 105

Henke, B. L., Gullikson, E. M. & Davis, J. C., 1993 Atomic Data and Nuclear Data Tables, Vol. 54, No. 2, p. 335

Loulergue, M. and Nussbaumer, H. 1973, A&A, 24, 209

Marrs, R. E., 1995 *Experimental Methods in the Physical Science, Atomic Molecular and Optical Physics: Charged Particles*, Vol. 29a, p. 391 (Academic Press, San Diego)

Parkinson, J. H. 1973, A&A, 24, 215

Phillips, K. J. H., Greer, C. J., Bhatia, A. K., Coffey, I. H., Barnsley, R. & Keenan, F. P. 1997, A &A, 324, 381

Raassen, A. J. J., Mewe, R., Audard, M., Güdel, M.,Behar, E., Kaastra, J. S., van der Meer, R. L. J., Foley, C. R. & Ness, J. -U. 2002, A&A, 389, 228

Saraph, H. E. 1972, Computer Phys. Comm., 3, 256

Savin, D. W., Beiersdorfer, P., Ló pez-Urritia, Decaux, V., Gullikson, E. M., Kahn, S. M., Liedahl, D. A., Reed, K. J., & Widmann, K. 1996, ApJ, 470, 73

Steffen, R. M. & Alder, K. *The Electromagnetic Interaction in Nuclear Spectroscopy*, edited by W. D. Hamilton (North Holland, New York, 1975) p.505

Utter, S. B., Brown, G. V., Beiersdorfer, P., Clothiaux, E. J., & Podder, N. K., 1999, Rev. Sci. Instrum., 70, 284

Vainshtein, L. A. & Safranova, U. I. 1985, Physica Scripta, 31, 519

Vogel, D. A. 1992, Ph. D. Thesis

Wargelin B. J. 1993, Ph. D. Thesis

Zhang, H. L., Sampson, D. H., & Clark, R. E. H., 1990, Phys. Rev. A, 41, 198

This manuscript was prepared with the AAS LaTeX macros v5.2.

Table 1. Summary of Wavelengths, Relative Intensities, and Polarizations of the Fe XVI X-ray Lines

Label	Wavelength (Å)		Transition	Relative Intensity				Polarization
	Experiment	FAC		Exp[a]	Exp[b]	FAC[c]	FAC[d]	FAC
1 (A)[e]	15.111(4)	15.107	$2p^6 3s\ J=1/2 - 2p_{1/2}2p^4_{3/2}3s_{1/2}3d_{5/2}\ J=3/2$	0.20(8)	0.22(6)	0.100	0.10	0.22
2a (B)[e]	15.19(2)	15.185	$2p^6 3p_{3/2}\ J=3/2 - 2s_{1/2}2p^6 3s^2\ J=1/2$	0.15(6)	0.16(9)	0.180	0.18	0
2b (B)[e]	15.210(4)	15.215	$2p^6 3s\ J=1/2 - 2p_{1/2}2p^4_{3/2}3s_{1/2}3d_{3/2}\ J=1/2$	1	1	1	1	0
3 (C)[e]	15.261(3)	15.276	$2p^6 3s\ J=1/2 - 2p_{1/2}2p^4_{3/2}3s_{1/2}3d_{5/2}\ J=3/2$			0.640	0.64	0.25
4	15.516(5)	15.533	$2p^6 3s\ J=1/2 - 2p^2_{1/2}2p^3_{3/2}3s_{1/2}3d_{5/2}\ J=3/2$	0.08(7)	0.15(5)	0.190	0.19	0.19
5	15.679(9)	15.703	$2p^6 3s\ J=1/2 - 2p^2_{1/2}2p^3_{3/2}3s_{1/2}3d_{3/2}\ J=3/2$		0.02(5)	0.040	0.04	-0.19
6a	17.37(1)	17.404	$2p^6 3s\ J=1/2 - 2p^2_{1/2}2p^3_{3/2}3s^2\ J=3/2$	0.10(4)	0.08(5)	0.010	0.02	-0.28
6b	17.395(4)	17.426	$2p^6 3d_{5/2}\ J=5/2 - 2p^2_{1/2}2p^3_{3/2}3s_{1/2}3d_{5/2}\ J=5/2$	0.19(5)	0.15(3)	0.010	0.02	-0.28
		17.430	$2p^6 3d_{3/2}\ J=3/2 - 2p_{1/2}2p^4_{3/2}3p^2_{3/2}\ J=3/2$			0.010		-0.30
6c	17.417(4)	17.439	$2p^6 3d_{5/2}\ J=5/2 - 2p^2_{1/2}2p^3_{3/2}3s_{1/2}3d_{5/2}\ J=7/2$	0.16(5)	0.12(3)	0.020	0.05	0.15
		17.449	$2p^6 3d_{3/2}\ J=3/2 - 2p^2_{1/2}2p^3_{3/2}3s_{1/2}3d_{3/2}\ J=3/2$			0.030		-0.07
7	17.447(4)	17.473	$2p^6 3p_{1/2}\ J=1/2 - 2p^2_{1/2}2p^3_{3/2}3s_{1/2}3p_{3/2}\ J=3/2$	0.17(4)	0.21(3)	0.008	0.06	0.19
		17.481	$2p^6 3d_{3/2}\ J=3/2 - 2p^2_{1/2}2p^3_{3/2}3s_{1/2}3d_{3/2}\ J=5/2$			0.020		0.07
		17.485	$2p^6 3p_{3/2}\ J=3/2 - 2p^2_{1/2}2p^3_{3/2}3s_{1/2}3p_{3/2}\ J=1/2$			0.032		0
8a	17.494(6)	17.513	$2p^6 3p_{1/2}\ J=1/2 - 2p^2_{1/2}2p^3_{3/2}3s_{1/2}3p_{1/2}\ J=1/2$	0.37(6)	0.35(7)	0.017	0.19	0
		17.516	$2p^6 3d_{5/2}\ J=5/2 - 2p^2_{1/2}2p^3_{3/2}3s_{1/2}3d_{3/2}\ J=7/2$			0.019		0.06
		17.535	$2p^6 3d_{5/2}\ J=5/2 - 2p^2_{1/2}2p^3_{3/2}3s_{1/2}3d_{5/2}\ J=5/2$			0.087		-0.002
		17.537	$2p^6 3p_{3/2}\ J=3/2 - 2p^2_{1/2}2p^3_{3/2}3s_{1/2}3p_{3/2}\ J=3/2$			0.024		-0.17
		17.541	$2p^6 3p_{1/2}\ J=1/2 - 2p^2_{1/2}2p^3_{3/2}3s_{1/2}3p_{3/2}\ J=5/2$			0.043		0.11
8b	17.510(4)	17.552	$2p^6 3p_{1/2}\ J=1/2 - 2p^2_{1/2}2p^3_{3/2}3s_{1/2}3p_{1/2}\ J=3/2$	0.17(5)	0.24(2)	0.030	0.03	0.04
9a	17.592(4)	17.619	$2p^6 3p_{3/2}\ J=3/2 - 2p^2_{1/2}2p^3_{3/2}3s_{1/2}3p_{3/2}\ J=7/2$		0.19(3)	0.180	0.18	-0.20
9b	17.612(6)	17.638	$2p^6 3p_{1/2}\ J=3/2 - 2p^2_{1/2}2p^3_{3/2}3s_{1/2}3p_{1/2}\ J=5/2$		0.11(3)	0.040	0.04	-0.03
9c	17.633(7)	17.656	$2p^6 3p_{1/2}\ J=1/2 - 2p^2_{1/2}2p^3_{3/2}3s_{1/2}3p_{1/2}\ J=3/2$		0.05(3)	0.020	0.02	0.04
10	17.678(3)	17.721	$2p^6 3p_{3/2}\ J=3/2 - 2p^2_{1/2}2p^3_{3/2}3s_{1/2}3p_{1/2}\ J=3/2$		0.20(2)	0.070	0.07	-0.03

[a]Crystal Spectrometer

[b]Grating Spectrometer

[c]Individual normalized line intensities

[d]Total line ratio for resolvable feature

[e]The 'A', 'B', and 'C' refer to Brown et al. (2001)

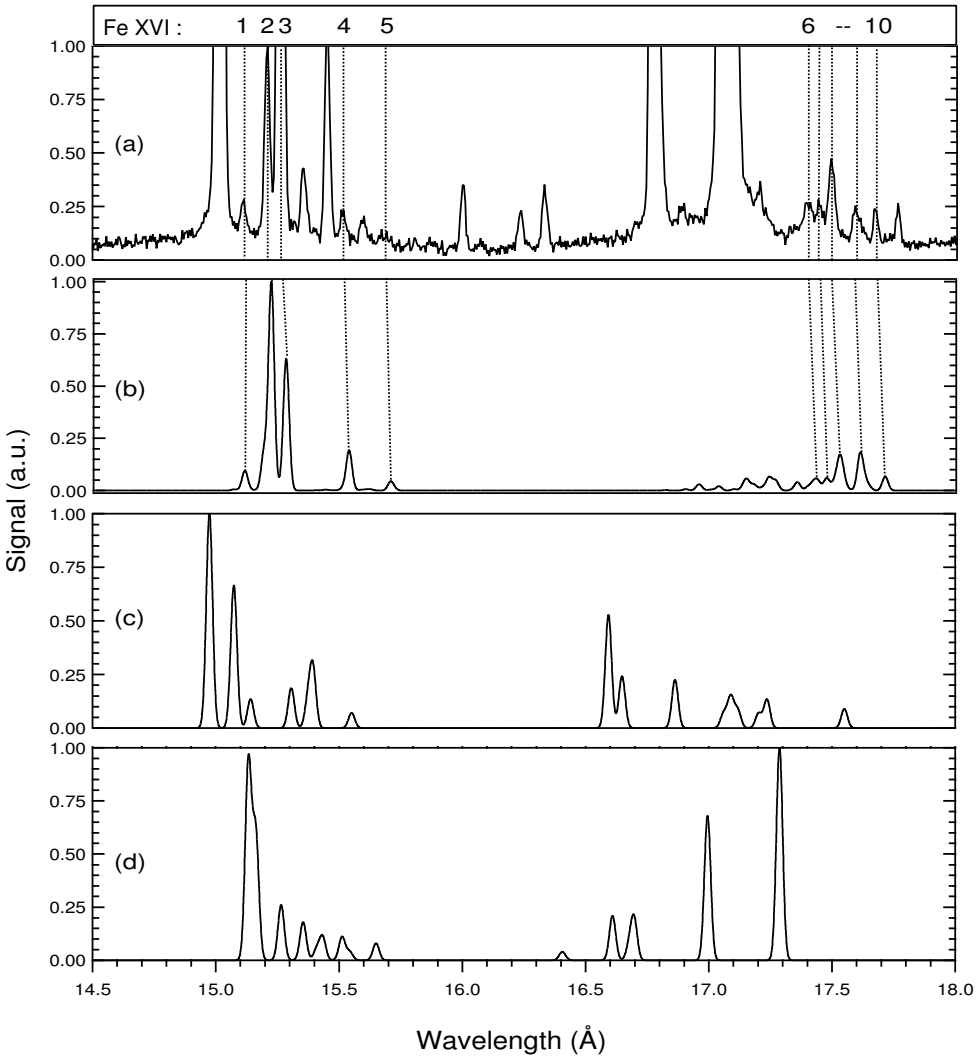

Fig. 1.— (a) Experimental spectrum at a beam energy of 1.1 keV. Dashed lines indicate the location of the Fe XVI inner-shell satellite features identified in Table 1. The numbers above the top graph refer to the labels used in Table 1. The saturated features belong to well known transitions in Fe XVII. (b) Theoretical results from FAC for a beam energy of 1.1 keV and a density $n_e = 3x10^{11} cm^{-3}$; (c) Theoretical results from Cornille et al. (1994) at 816 eV and $n_e < 10^{12} cm^{-3}$; (d) Theoretical results from Phillips et al. (1997) at 843 eV and $n_e = 10^8\ cm^{-3}$.

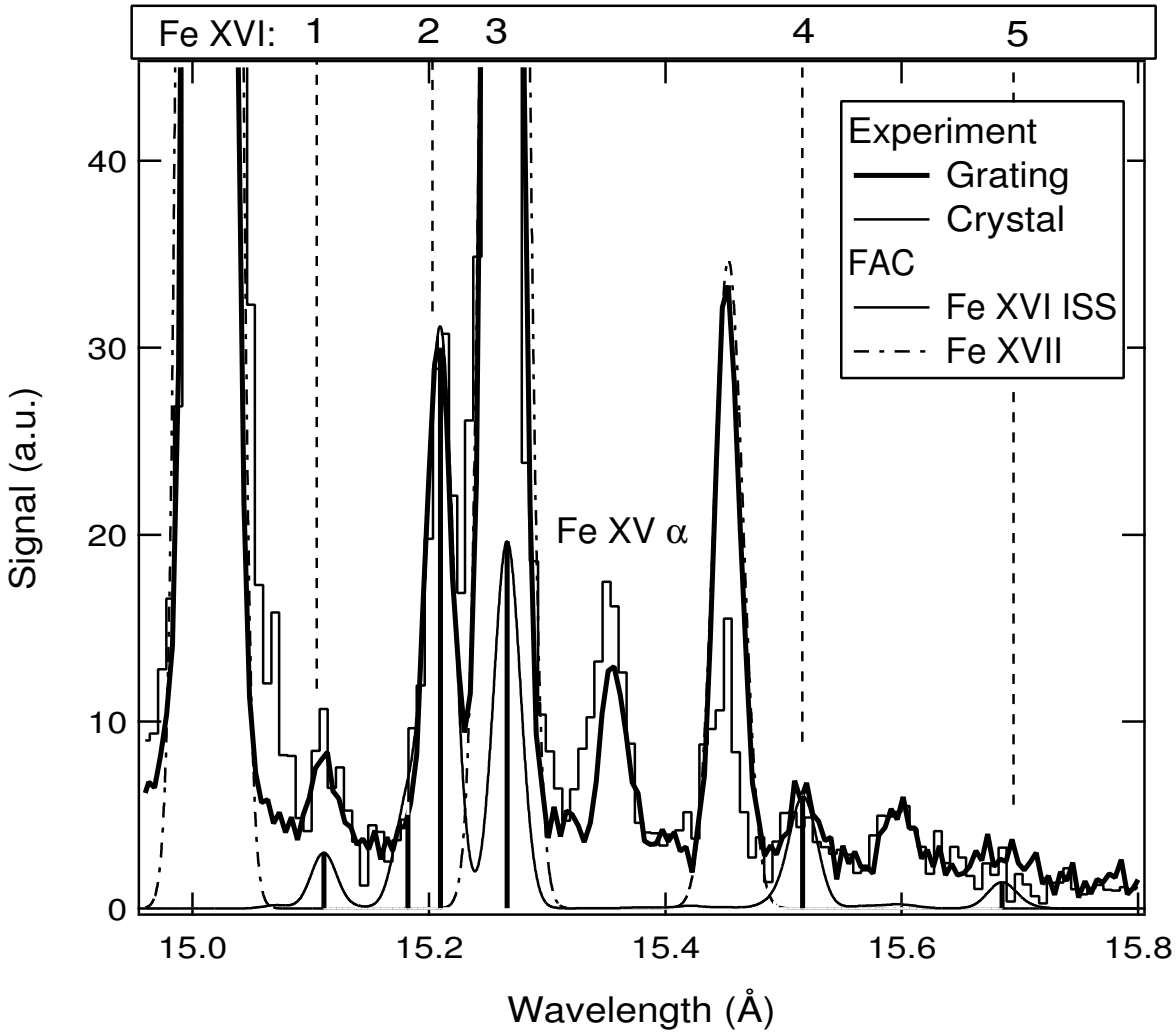

Fig. 2.— Comparison of results from the crystal spectrometer, the grating spectrometer, and the calculated spectrum from FAC between 15.09 and 15.54 Å. The FAC calculations include emission from Fe XVII and IS satellites from Fe XVI. The FAC wavelength values have been shifted by as much as 50 mÅ to preserve clarity for this plot. The spectra are normalized to line 2 at 15.20 Å. The experimental data shown include only broadband corrections to the intensity, i.e., no correction for polarization effects.

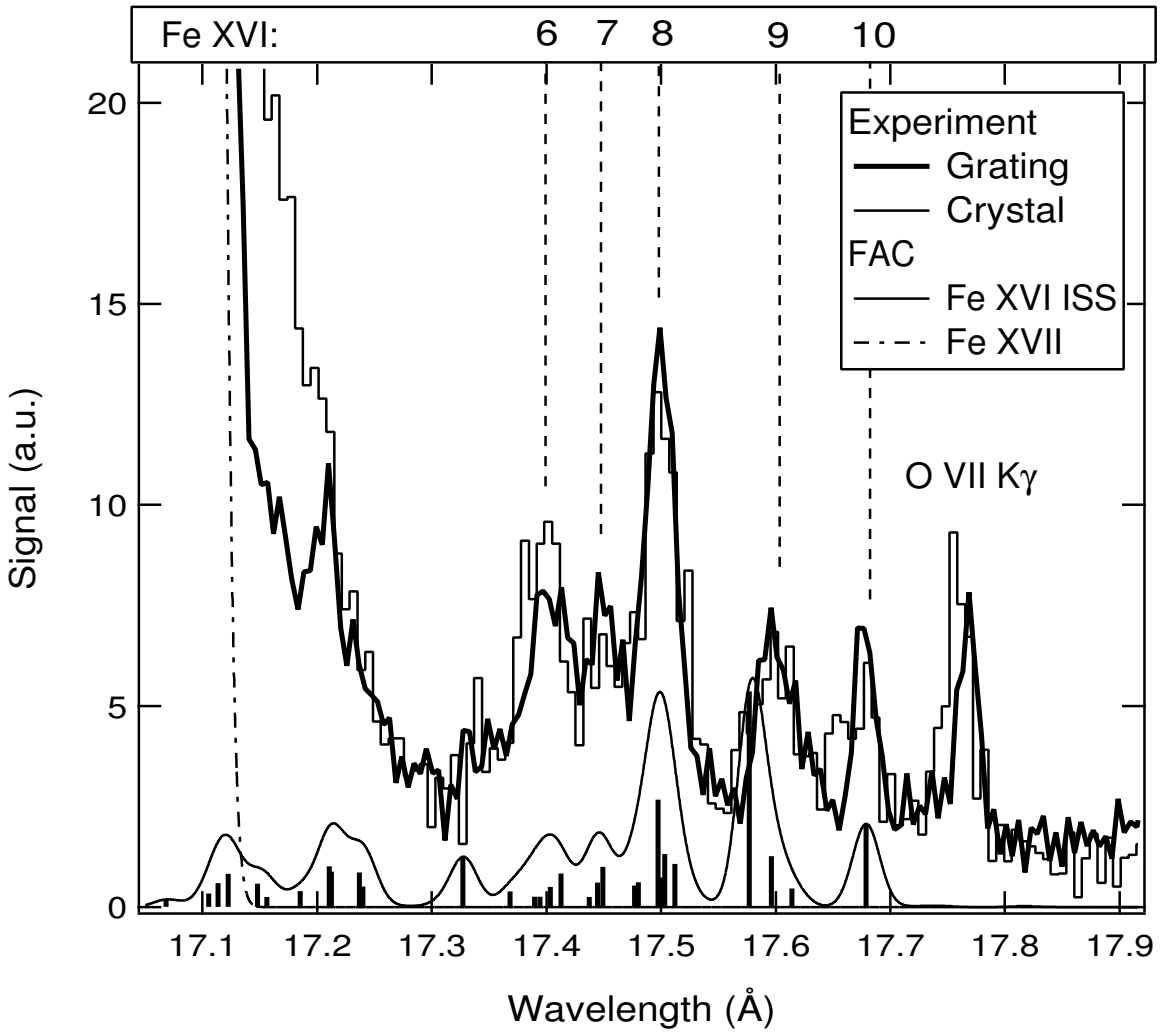

Fig. 3.— Comparison of experimental data around 17.4 Å from the crystal spectrometer, the grating spectrometer and the calculated spectrum from FAC. The FAC wavelength values have been shifted by as much as 50 mÅ to preserve clarity for this plot. The Fe XVI line intensity is normalized to 2 at 15.20 Å. The experimental data shown include only broadband corrections to the intensity. We also note the contamination from O VII K_δ and K_γ at 17.396 and 17.768 Å, respectively.

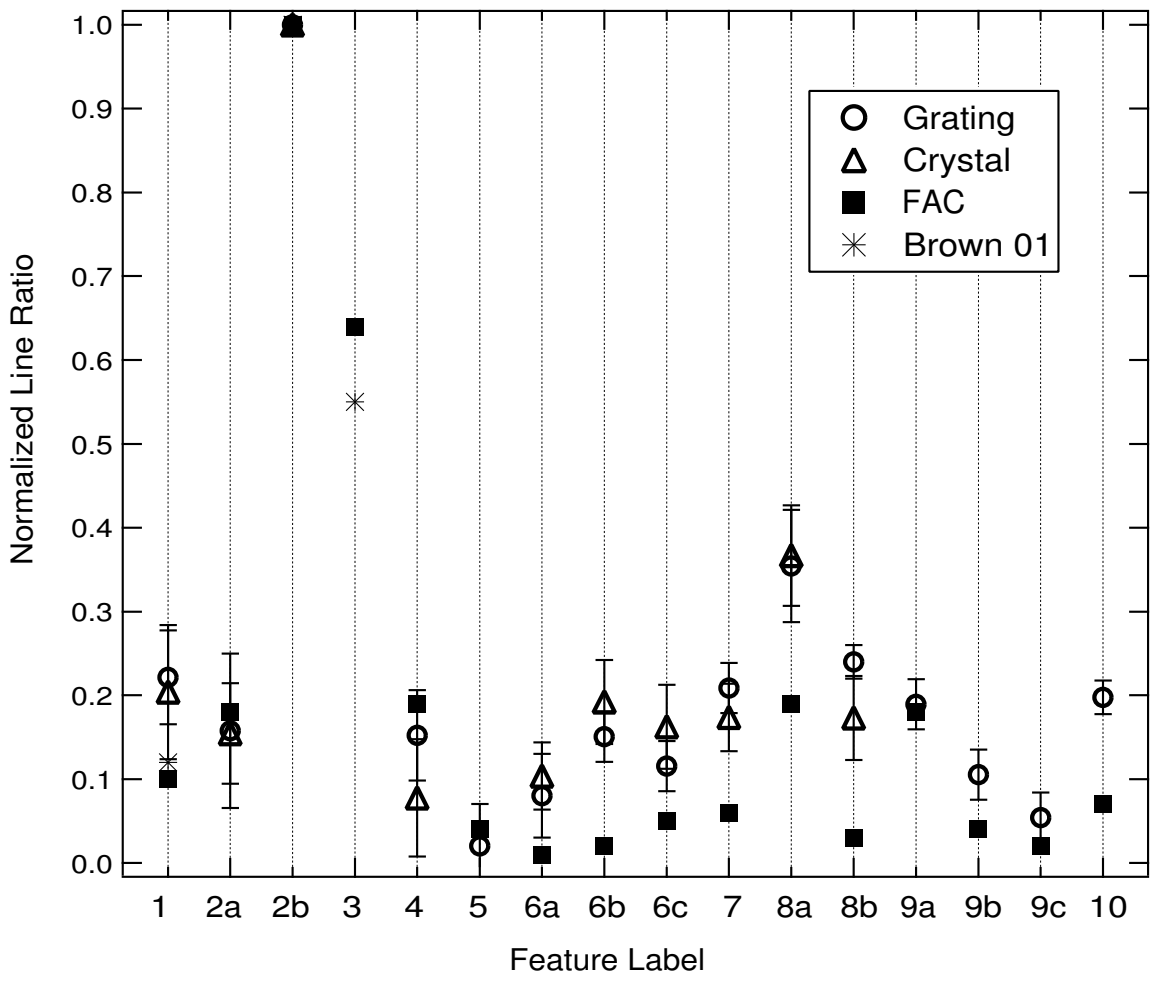

Fig. 4.— Line intensities of Fe XVI IS satellites relative to line 2 at 15.20 Å. The squares are taken from the calculated spectrum produced by FAC. The triangles are from the crystal spectrometer. The circles are from the grating spectrometer. The stars are from Brown et al. (2001). The feature labels refer to those in Table 1.